Nano Research 2014, 7(11): 1631–1639
DOI 10.1007/s12274-014-0523-y
Research Article

ISSN 1998-0124
CN 11-5974/O4

Hybrid energy cell for simultaneously harvesting wind, solar, and chemical energies

Yingchun Wu[1], Xiandai Zhong[1], Xue Wang[1], Ya Yang[1] (✉), and Zhong Lin Wang[1,2] (✉)

[1] *Beijing Institute of Nanoenergy and Nanosystems, Chinese Academy of Sciences, Beijing 100083, China*
[2] *School of Materials Science and Engineering, Georgia Institute of Technology, Atlanta, Georgia 30332-0245, USA*

Received: 21 May 2014
Revised: 15 June 2014
Accepted: 23 June 2014

KEYWORDS
hybrid energy cell, wind energy, solar energy, triboelectric nanogenerators, electrochemical cells

ABSTRACT

We report a hybrid energy cell that can simultaneously or individually harvest wind, solar, and chemical energies to power some electronic devices. By utilizing the wind driven relative rotations between a polytetrafluoroethylene film and an etched Al film attached on two acrylic tubes, the fabricated triboelectric nanogenerator (TENG) can deliver an open-circuit voltage of about 90 V, a short-circuit current density of about 0.5 mA/m^2, and a maximum power density of 16 mW/m^2, which is capable of directly lighting up 20 blue light-emitting-diodes (LEDs). By integrating a TENG, a solar cell, and an electrochemical cell, a hybrid energy cell has been fabricated to simultaneously scavenge three different types of energies. As compared with the individual energy units, the hybrid energy cell exhibited much better performance in charging a capacitor. Moreover, we also demonstrated that the hybrid energies generated can be stored in a Li-ion battery for powering a commercial wind speed sensor and a temperature sensor. This work represents significant progress toward practical applications of hybrid energy cells, providing potential solutions for simultaneously scavenging wind, solar, and chemical energies.

1 Introduction

Harvesting wind, solar, and chemical energies from the environment have attracted increasing attention in the past decade due to the growing energy crisis and global warming [1–3]. However, these energies are not always available at the same time, depending on the light, the weather, and other conditions. The purpose of developing hybrid energy cells is to simultaneously/individually harvest these energies by designing an integrated device [4–6], so that the devices can utilize whatever type of energy is available [7]. Although some hybrid energy cells for harvesting two kinds of energies have been demonstrated, there has been no report of a hybrid energy cell that can simultaneously scavenge wind, solar, and chemical energies. It is necessary to simultaneously scavenge these energies to realize the maximum utilization

Address correspondence to Ya Yang, yayang@binn.cas.cn; Zhong Lin Wang, zlwang@gatech.edu

of energy from the environment, and to achieve stable electrical energy output. Conventional wind energy generators usually are based on the electromagnetic and piezoelectric effects [8–10]. Triboelectric nanogenerators (TENGs) have been developed for scavenging the mechanical energy from impacts, sliding, and rotations [11–15]. The recent invention of single-electrode based TENGs has expanded potential applications further, and decreased the fabrication cost of the devices due to there being no need to deposit metal electrodes on the triboelectric materials for effective electrical output, allowing them to be utilized in wind energy harvesting [16]. Currently, many kinds of solar cells have been fabricated for harvesting solar energy [17–19]. Electrochemical cells convert chemical energy to electricity by using the spontaneous oxidation–reduction reactions at two different metal electrodes in an electrolyte solution to drive electrons to flow in an external circuit [20], and sea water can be used as the electrolyte solution. Developing hybrid energy cells with low cost and multi-functionalities is of critical importance for advancing the practical applications of energy harvesting technologies.

In this work, we report a hybrid energy cell that can simultaneously or individually harvest wind, solar, and chemical energies to power some electronic devices. The hybrid energy cell consists of a TENG, a solar cell (SC), and an electrochemical cell (EC), where the SCs and ECs are connected in series. By utilizing the coupling between the triboelectric effect and the electrostatic effect, the periodic contact/separation between the Al film and the polytetrafluoroethylene (PTFE) film can induce charge transfer between the Al electrode and the ground, resulting in the flow of the electrons across an external loading resistor. The fabricated TENG can deliver an open-circuit voltage of about 90 V and a short-circuit current density of about 0.5 mA/m^2, which can be used to directly drive tens of blue light-emitting diodes (LEDs). The hybrid energy cell exhibited much better performance than that of individual energy units when charging a capacitor. We have also demonstrated that the hybrid energy cell can be utilized to charge a commercial Li-ion battery as a regulated power module for powering a wind speed sensor and a temperature sensor. This work represents important progress toward the practical applications of wind, solar, and chemical energy harvesting techniques.

2 Experimental

2.1 Fabrication of the hybrid energy cell

The TENG consists of a PTFE film and an Al film attached to two transparent cylindrical acrylic tubes. The surface of the Al film was etched into nanostructures by using a simple method, whereby the Al film was immersed in hot deionized water at 120 ℃ for 20 min. The SC unit consists of eight amorphous silicon-based solar cells in series with the total dimensions 30 mm × 60 mm × 3.2 mm. The EC unit was fabricated by utilizing the Al film electrode, NaCl solution (about 3 wt.%), and a Cu film electrode attached to a transparent glass container. The SC and EC units are placed on, and in, the TENG, respectively.

2.2 Measurement of the fabricated hybrid energy cell

The output voltage and current of the hybrid energy cell were measured by a Keithley 6514 System Electrometer and a low-noise current preamplifier (Stanford Research SR570), respectively.

3 Results and discussion

Figure 1(a) illustrates a schematic diagram of a fabricated hybrid energy cell, where the silicon-based SC units were fabricated on the top for harvesting solar energy. The TENG consists of a PTFE film and an Al film attached to two transparent cylindrical acrylic tubes. The periodical contact and separation between the PTFE film and the Al film can be created by the wind-induced rotation of the outer acrylic tube, resulting in electron transfer between the Al film and the ground. As shown in the inset of Fig. 1(a), the EC unit with the electrodes of Cu and Al films was placed in the inner acrylic tube of the TENG. Figure 1(b) depicts a photograph of a hybrid energy cell, where the SC and EC units are placed on, and in, the TENG, respectively. Usually, the output

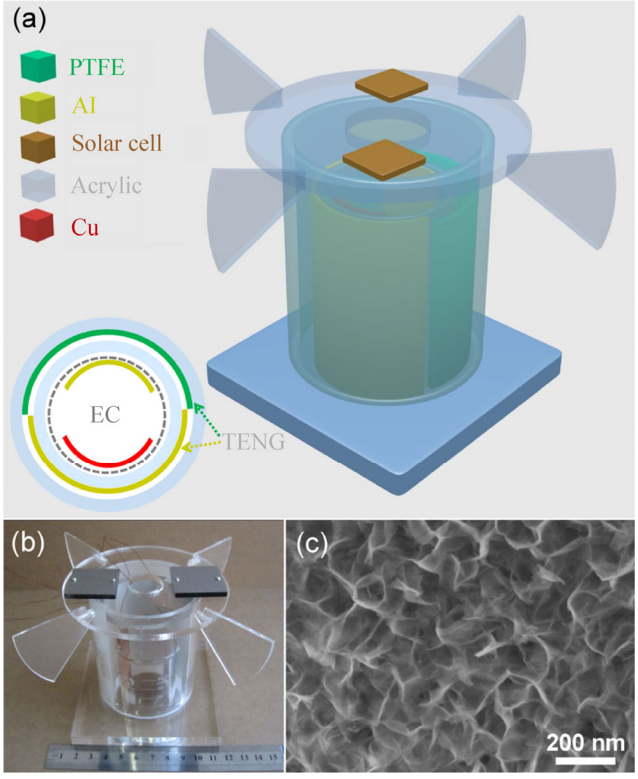

Figure 1 (a) Schematic diagram of the fabricated hybrid energy cell. The inset shows the cross-sectional schematic diagram of the device. (b) Photograph of the fabricated hybrid energy cell, where the solar cells and electrochemical cells can be placed on and in the TENG, respectively. (c) SEM image of Al film surface modified with nanostructures.

performance of a TENG can be enhanced by increasing the surface roughness and the effective surface area of the triboelectric material in order to induce a larger triboelectric charge density [13]. In this study, to increase the effective surface area of the Al film, the surface of the Al film was etched into nanostructures by using a simple method, whereby the Al film was immersed in hot deionized water at 120 ℃ for 20 min. Figure 1(c) presents a SEM image of the etched Al film, which is uniformly covered by nanostructures with dimensions smaller than 200 nm.

The working mechanism of the TENG is schematically illustrated in Fig. 2 and involves the coupling of contact electrification and electrostatic induction. At the aligned position, the surfaces of the two Al and PTFE films fully contact with each other, which can induce the electron transfer from Al to PTFE and result in opposite charges being created on the surfaces of the two films according to the triboelectric

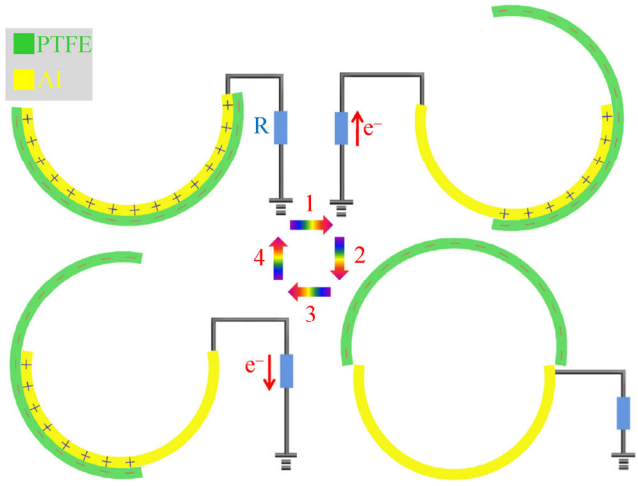

Figure 2 Sketches that illustrate the electricity generation process in a full cycle.

series [21]. Since the resulting triboelectric charges with opposite polarities are fully balanced, there is no electron flow between the Al film and the ground. Once a relative sliding between the Al film and the PTFE film occurs due to the wind driven rotation of the outer acrylic tube, the triboelectric charges cannot be compensated, resulting in electrons flowing from the ground to the Al film. The flow of the electrons can last until the mismatch between the Al and PTFE films reaches a maximum, as displayed in Fig. 2. As the relative rotation between the Al and PTFE films continues, the PTFE film slides back to contact the Al film, resulting in the reversed flow of electrons from the Al to the ground. This electrostatic induction process can produce output signals until the negative triboelectric charges on the PTFE film are fully screened from the induced positive charges on the Al film. Thus, an alternating electric (AC) output can be generated in the cycle of electricity generation.

The electric potential distribution and the charge transfer between the Al film and the ground was verified through finite element simulation using COMSOL. The constructed model consists of a PTFE film and an Al film with a thickness of 2 mm, where the Al film was connected with the ground. The triboelectric charge density on the surface of the PTFE film was assumed to be –10 μC/m^2. Figure 3(a) displays the calculated results of the electric potential distribution in the TENG with different rotation angles of 0°, 90°, and 180°, respectively. The largest

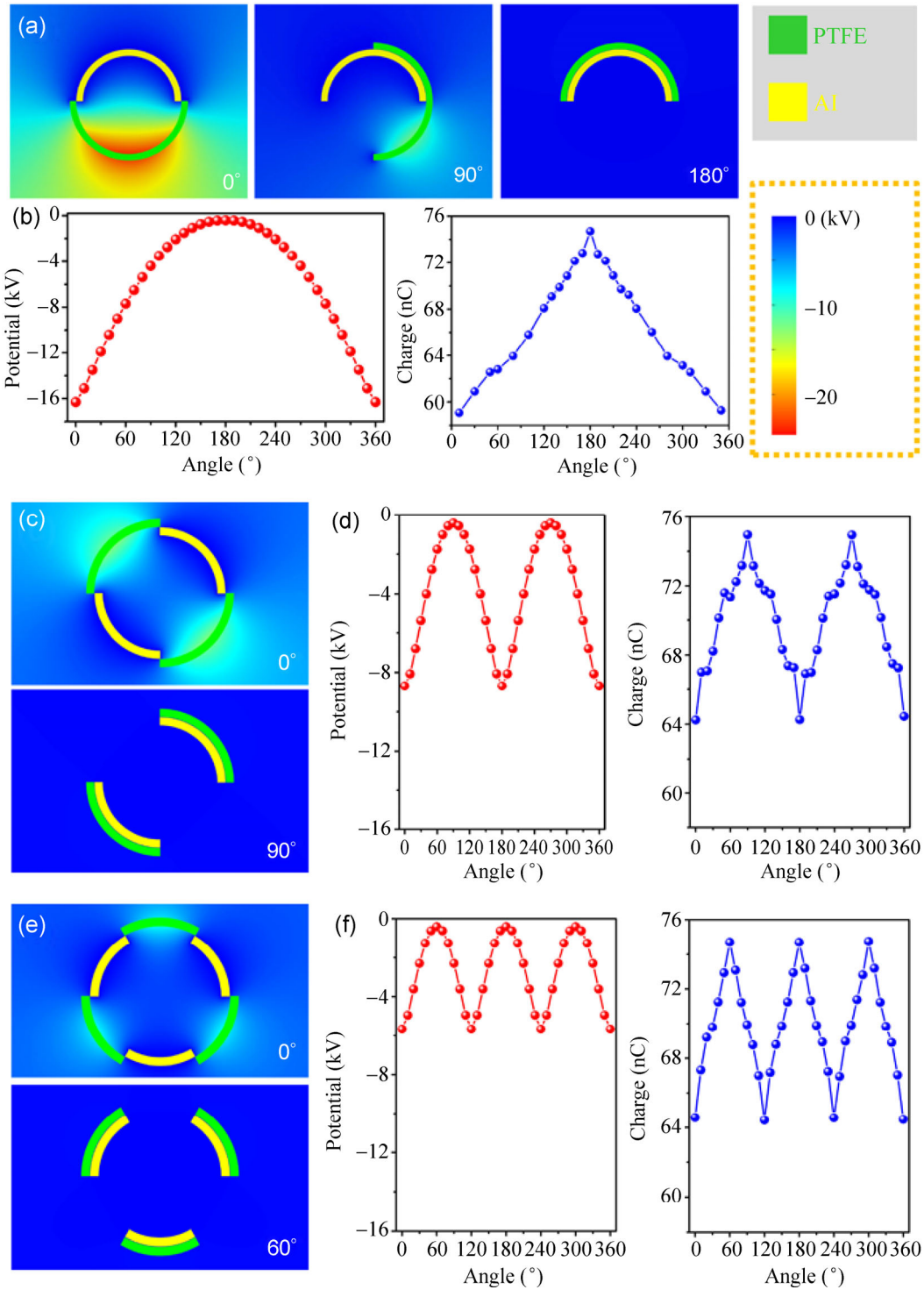

Figure 3 (a) Electric potential distribution in the TENG with one strip unit at the rotation angles of 0°, 90°, and 180°. (b) Average electric potential on the PTFE film under the different rotation angles and the total charge amount on the Al film of the TENG in (a). Electric potential distribution (c) in the TENG with two strip units and the changes (d) in the electric potential on the PTFE film and the charge amount on the Al film with increasing the rotation angles. Electric potential distribution (e) in the TENG with three strip units and the changes (f) in the electric potential on the PTFE film and the charge amount on the Al film with increasing the rotation angles.

average potential on the PTFE film can be up to –16 kV when the two films were fully mismatched. The potential has the smallest value at a rotation angle of 180°, and was found to dramatically increase with increasing/decreasing rotation angles, as depicted in Fig. 3(b). The amount of the total charges on the Al film increased with increasing rotation angle when smaller than 180° and then decreased on further increasing the angle. The amount of charge transferred between the Al film and the ground has the largest value at a rotation angle of 180°. We also calculated the electric potential distribution and the amount of charge on the Al film for the two and three strip units of both the Al film and PTFE film, as illustrated Figs. 3(c)–3(f). The results indicate that the change in the amount of charge on the Al film decreased with increasing the number of strips. However, under the same rotation speeds, the cycle time of the contact and separation between the Al and PTFE films markedly decreased with increasing number of strips, resulting in the TENG having larger instantaneous output current for a larger number of strip units according to the current equation ($I = \Delta Q / \Delta T$), where the ΔQ is the amount of charge transferred between the Al film and the ground in the time of ΔT.

Figure 4(a) shows the measured open-circuit voltage and short-circuit current density of the fabricated TENG with one strip unit, where the voltage and current density are about 90 V and 0.5 mA/m^2, respectively. Under a loading resistance of 100 MΩ, the output voltage and current density of the TENG decrease to about 40 V and 0.25 mA/m^2, respectively, as displayed in Fig. 4(b). Usually, the effective output power of the TENG depends on the match with the loading resistance. Figure 4(c) presents the resistance dependence of both output voltage and current density, with the resistance ranging from 10 Ω to 1 GΩ, based on an analysis of 30 peak signals. The output voltage of the TENG was found to increase with increasing loading resistance, while the current density decreased with the increase of the resistance. Figure 4(d) shows the output power density as a function of the loading resistance. The instantaneous power density was found to initially increase with increasing loading resistance (< 100 MΩ) and then decrease under larger loading resistance. The maximum value of the output power density can reach about 16 mW/m^2 at a loading resistance of 100 MΩ. Figures 4(e) and 4(f) show the output voltage is about 50 V and the current density is about 0.4 mA/m^2 for the TENG with the two strip units of both the Al film and PTFE film under a loading resistance of 100 MΩ. The corresponding instantaneous power density is about 20 mW/m^2, which is larger than that of the TENG with one strip unit (16 mW/m^2) in Fig. 4(b), indicating that the output power can be enhanced by increasing the number of strip units.

Figures 5(a) and 5(b) display an output current of about 500 μA and an output voltage of about 4 V for 8 SC units in series, respectively. The fabricated EC consists of a Cu electrode, the NaCl solution (about 3 wt.%), and an Al electrode. The spontaneous oxidation–reduction reactions in the NaCl solution can drive electrons to flow in the external circuit, resulting in the observed output signals. Figures 5(c) and 5(d) show the output current and voltage of the EC unit under forward and reversed connections to the electrical measurement system, respectively. The measured current and voltage are about 6.5 mA and 0.5 V, respectively. The obvious current peak is associated with the charge–discharge process of the capacitor induced by the ON/OFF switch in the circuit. After connecting the SC and EC units in series, Figs. 5(e) and 5(f) show that the total output current and voltage are about 500 μA and 4.5 V, respectively. To illustrate the potential applications of the hybrid energy cell as a power source, the TENG and SC+EC units were connected with 20 blue LEDs in series and 20 red LEDs in parallel, respectively, as illustrated in Fig. 6(a). The 20 blue LEDs were divided into two groups in series, which were connected to the TENG with reversed polarity. The blue and red LEDs can be lit up when the TENG and the SC+EC units, respectively, are working. All the LEDs can be lit up when the wind, solar and chemical energies are simultaneously scavenged. Figure 6(b) displays the hybrid output voltage of the TENG and SC+EC units in series, where the output voltage signals of the TENG were rectified by using a bridge rectification circuit. It can be seen that the TENG and SC+EC units can work simultaneously and individually to harvest the different energies. The output voltage

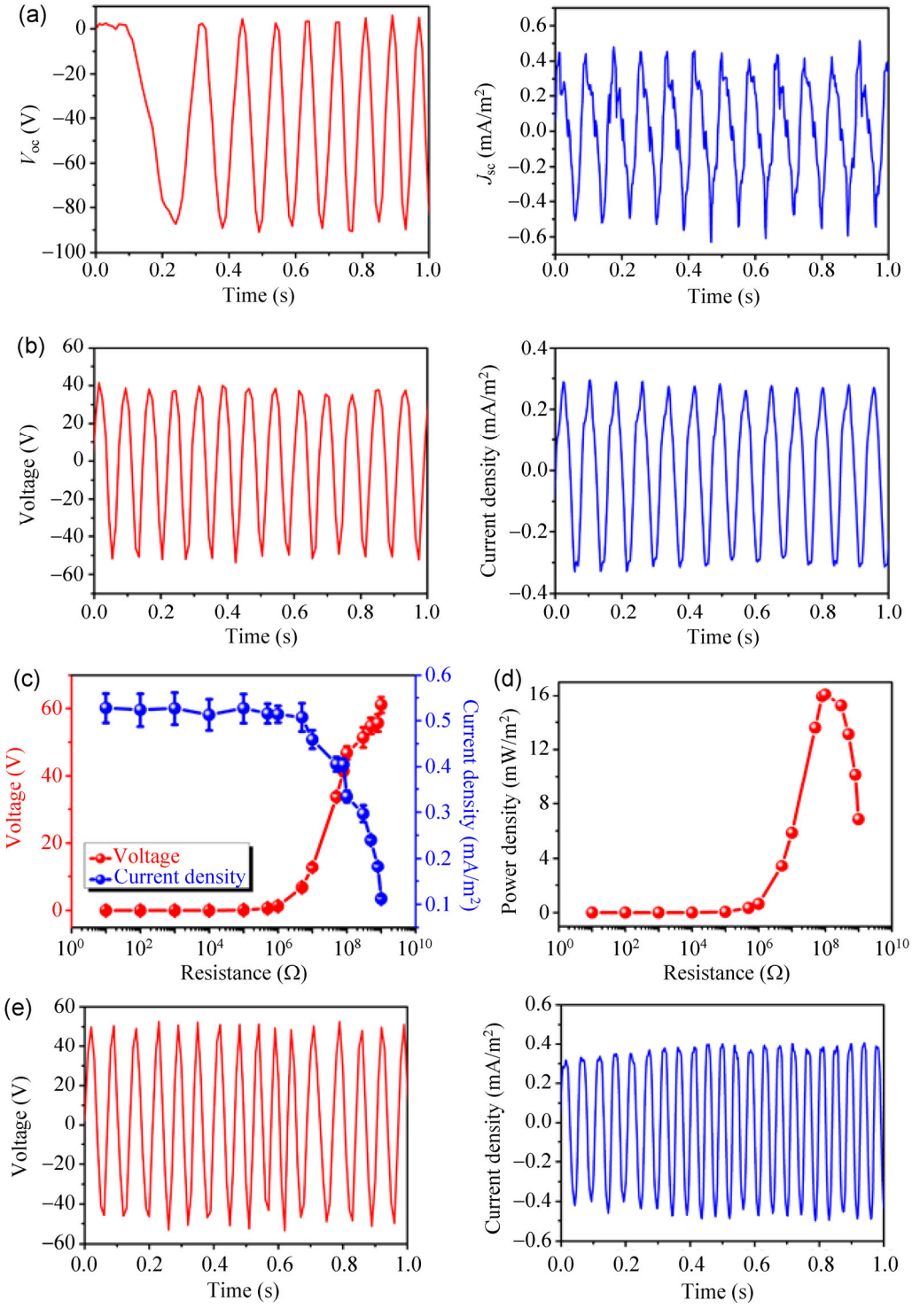

Figure 4 (a) Open-circuit voltage and short-circuit current density of the TENG with one strip unit. (b) Measured output voltage and current density of the TENG with one strip unit under the loading resistance of 100 MΩ. (c) Dependence of the output voltage and current density on the external loading resistance by the analysis of 30 output peak signals. (d) Plot of the power density versus the loading resistance. (e) Measured output voltage and current density of the TENG with two strip units.

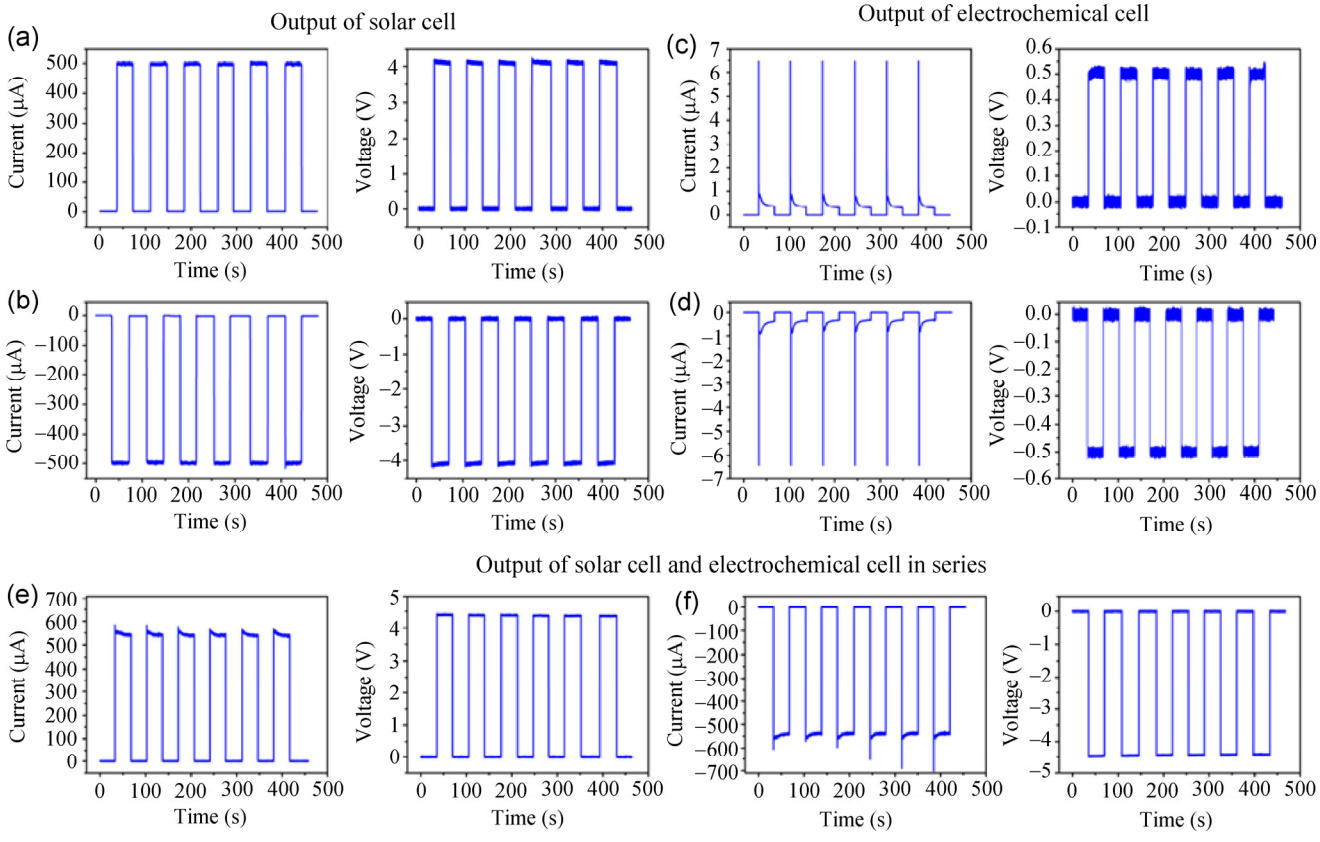

Figure 5 Measured output current and voltage of the solar cell units under forward (a) and reversed (b) connections to the electrical measurement system. Measured output current and voltage of the electrochemical cell under forward (c) and reversed (d) connections. Measured output current and voltage of the hybrid solar cell and electrochemical cell in series under forward (e) and reversed (f) connections.

of the TENG is much larger than that of the SC+EC units. Figure 6(c) shows the hybrid output current of the TENG and SC+EC units in parallel, indicating that the output current of the TENG is smaller than that of the SC+EC units, as illustrated in the inset.

To demonstrate more potential applications of the hybrid energy cell, it is necessary to store the produced energy by utilizing some energy storage units such as capacitors or Li-ion batteries. Figure 6(d) illustrates the charging curves of the TENG, SC+EC, and TENG// (SC+EC) units for charging a capacitor of 10 μF. For the same charging time, the highest charging voltage can be found for TENG//(SC+EC) units as compared with the TENG and SC+EC units, indicating that the fabricated hybrid energy cell has much better charging performance than that of individual energy units. Figure 7(a) shows the hybrid energy cell-charging and the subsequent constant-current discharging curves of a Li-ion battery. The battery can be charged by the hybrid energy cell from 1.1 to 3.0 V in about 7,500 s. Under a constant discharging current of 1 mA, the discharging of the charged Li-ion battery can last for about 0.35 h before the voltage decreases to the original value of 1.1 V. Thus, the stored electrical capacity is about 0.35 mAh. Figure 6(b) shows that the Li-ion battery can be used to power a wind speed sensor and a temperature sensor. By using the Li-ion battery driven sensors, the measured wind speed and temperature are about 28.6 mph and 71.8 °F, respectively, as shown in Figs. 6(c) and 6(d). These results indicate that the hybrid energy cell has the potential applications as a way of charging a Li-ion battery for powering personal electronic devices.

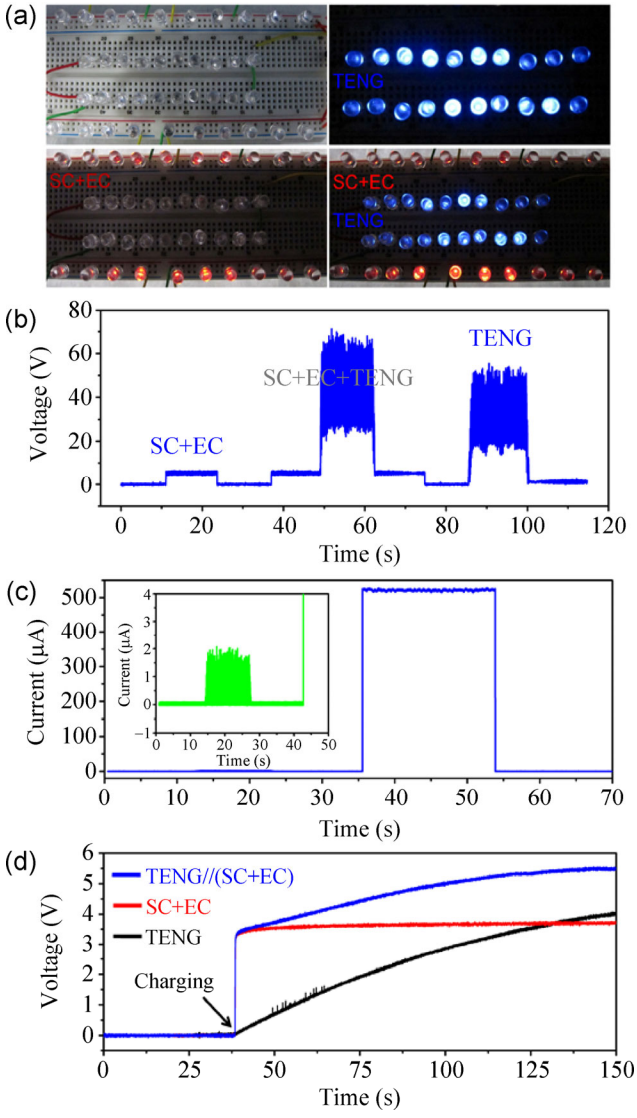

Figure 6 (a) Optical images of 40 LEDs (20 red LEDs for SC+EC; 20 blue LEDs for TENG). (b) Output voltage of the SC+EC, TENG (after rectification), and the hybrid energy cell (SC+EC and TENG in series). (c) Output current of the hybrid energy cell (SC+EC and TENG in parallel). The inset shows the enlarged current curve produced by the TENG. (d) The measured voltage of a 10 μF capacitor charged by the TENG, SC+EC, and the hybrid energy cell (SC+EC and TENG in parallel).

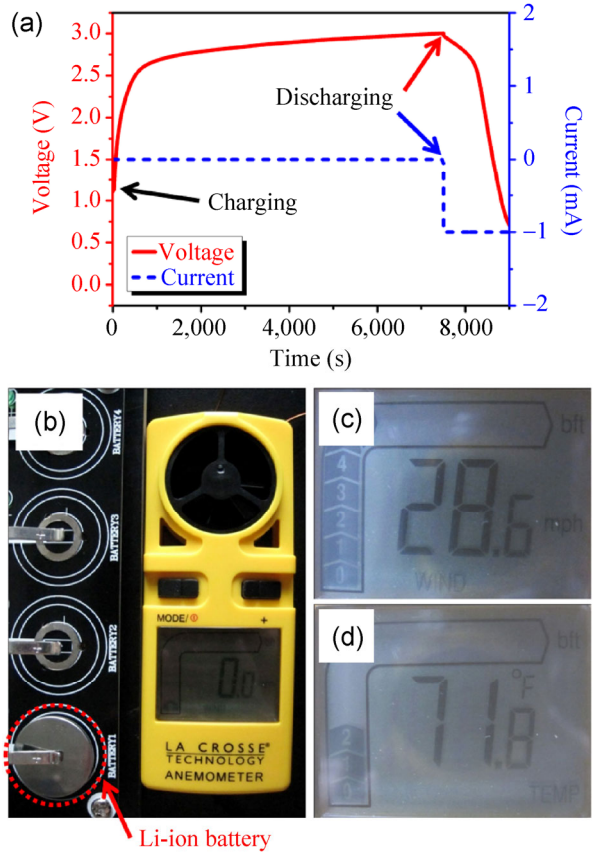

Figure 7 (a) Voltage curve showing the entire cycle of a Li-ion battery charged by the hybrid energy cell, with the subsequent constant current discharge at 1 mA. (b) Optical image of the wind speed and temperature sensors powered by the charged Li-ion battery. Optical images of the working wind speed sensor (c) and the working temperature sensor (d).

4 Conclusion

We have demonstrated a hybrid energy cell that consists of a TENG, a SC, and an EC, which can be used to simultaneously/individually harvest wind, solar and chemical energies. The TENG was designed by using a PTFE film and an Al film attached to two transparent cylindrical acrylic tubes. The mechanism of the TENG is based on the charge transfer between the Al electrode and ground by utilizing the wind driven relative rotation between the PTFE and Al films. The fabricated TENG can produce an open-circuit voltage of about 90 V and a short-circuit current density of about 0.5 mA/m^2, which can be used to directly light up tens of blue LEDs. When charging a capacitor, the hybrid energy cell exhibited better charging performance than that of the individual energy harvesting units. The hybrid energy cell has also been used to build up a power module together with a Li-ion battery for driving some personal electronic devices such as a wind speed sensor and a temperature sensor. This invention of hybrid energy cells may be a significant step toward the practical applications of wind, solar and chemical energy harvesting techniques.

Acknowledgements

We thank the Chinese "Thousands Talents" Program for Pioneer Researchers and Their Innovation Teams, for support.

References

[1] McElroy, M. B.; Lu, X.; Nielsen, C. P.; Wang, Y. X. Potential for wind-generated electricity in China. *Science* **2009**, *325*, 1378–1380.

[2] Lewis, N. S. Toward cost-effective solar energy use. *Science* **2007**, *315*, 798–801.

[3] Long, R. Production and utilization of chemical energy. *Nature* **1950**, *166*, 669–672.

[4] Yang, Y.; Zhang, H. L.; Lee, S. M.; Kim, D.; Hwang, W.; Wang, Z. L. Hybrid energy cell for degradation of methyl orange by self-powered electrocatalytic oxidation. *Nano Lett.* **2013**, *13*, 803–808.

[5] Han, M. D.; Zhang, X. S.; Meng, B.; Liu, W.; Tang, W.; Sun, X. M.; Wang, W.; Zhang, H. X. r-Shaped hybrid nanogenerator with enhanced piezoelectricity. *ACS Nano* **2013**, *7*, 8554–8560.

[6] Yang, Y.; Zhang, H. L.; Liu, Y.; Lin, Z. H.; Lee, S.; Lin, Z. Y.; Wong, C. P.; Wang, Z. L. Silicon-based hybrid energy cell for self-powered electrodegradation and personal electronics. *ACS Nano* **2013**, *7*, 2808–2813.

[7] Yang, Y.; Zhang, H. L.; Zhu, G.; Lee, S.; Lin, Z. H.; Wang, Z. L. Flexible hybrid energy cell for simultaneously harvesting thermal, mechanical, and solar energies. *ACS Nano* **2013**, *7*, 785–790.

[8] Priya, S.; Chen, C. T.; Fye, D.; Zahnd, J. Piezoelectric windmill: A novel solution to remote sensing. *Jpn. J. Appl. Phys.* **2005**, *44*, L104–L107.

[9] Priya, S. Modeling of electric energy harvesting using piezoelectric windmill. *Appl. Phys. Lett.* **2005**, *87*, 184101.

[10] Myers, R.; Vickers, M.; Kim, H.; Priya, S. Small scale windmill. *Appl. Phys. Lett.* **2007**, *90*, 054106.

[11] Wang, S. H.; Lin, L.; Wang, Z. L. Nanoscale triboelectric-effect-enabled energy conversion for sustainably powering portable electronics. *Nano Lett.* **2012**, *12*, 6339–6346.

[12] Zhang, X. S.; Han, M. D.; Wang, R. X.; Zhu, F. Y.; Li, Z. H.; Wang, W.; Zhang, H. X. Frequency-multiplication high-output triboelectric nanogenerator for sustainably powering biomedical microsystems. *Nano Lett.* **2013**, *13*, 1168–1172.

[13] Yang, Y.; Zhang, H. L.; Chen, J.; Jing, Q. S.; Zhou, Y. S.; Wen, X. N.; Wang, Z. L. Single-electrode-based sliding triboelectric nanogenerator for self-powered displacement vector sensor system. *ACS Nano* **2013**, *7*, 7342–7351.

[14] Xie, Y. N.; Wang, S. H.; Lin, L.; Jing, Q. S.; Lin, Z. H.; Niu, S. M.; Wu, Z. Y.; Wang, Z. L. Rotary triboelectric nanogenerator based on a hybridized mechanism for harvesting wind energy. *ACS Nano* **2013**, *7*, 7119–7125.

[15] Zhang, H. L.; Yang, Y.; Zhong, X. D.; Su, Y. J.; Zhou, Y. S.; Hu, C. G.; Wang, Z. L. Single-electrode-based rotating triboelectric nanogenerator for harvesting energy from tires. *ACS Nano* **2014**, *8*, 680–689.

[16] Yang, Y.; Zhu, G.; Zhang, H. L.; Chen, J.; Zhong, X. D.; Lin, Z. H.; Su, Y. J.; Bai, P.; Wen, X. N.; Wang, Z. L. Triboelectric nanogenerator for harvesting wind energy and as self-powered wind vector sensor system. *ACS Nano* **2013**, *7*, 9461–9468.

[17] McGehee, M. D. Paradigm shifts in dye-sensitized solar cells. *Science* **2011**, *334*, 607–608.

[18] Kempa, T. J.; Tian, B.; Kim, D. R.; Hu, J. S.; Zheng, X. L.; Lieber, C. M. Single and tandem axial p–i–n nanowire photovoltaic devices. *Nano Lett.* **2008**, *8*, 3456–3460.

[19] Lin, Y. Y.; Lee, Y. Y.; Chang, L. W.; Wu, J. J.; Chen, C. W. The influence of interface modifier on the performance of nanostructured ZnO/polymer hybrid solar cells. *Appl. Phys. Lett.* **2009**, *94*, 063308.

[20] Bresadola, M. Medicine and science in the life of Luigi Galvani. *Brain Res. Bull.* **1998**, *46*, 367–380.

[21] Wang, Z. L. Triboelectric nanogenerators as new energy technology for self-powered systems and as active mechanical and chemical sensors. *ACS Nano* **2013**, *7*, 9533–9557.